PERGAMON

International Journal of Heat and Mass Transfer 43 (2000) 3469–3480

International Journal of HEAT and MASS TRANSFER

www.elsevier.com/locate/ijhmt

Effect of porous media transparency on spherical and cylindrical filtrational combustion heaters performance

S.A. Zhdanok*, K.V. Dobrego, S.I. Futko

Luikov Heat and Mass Transfer Institute, 15 P. Brovki Street, Minsk 220033, Belarus

Received 8 June 1998

Abstract

An influence of partial transparency of a porous media on radiative efficiency, maximum solid phase temperature and combustion localization radius of cylindrical and spherical filtration heater has been investigated by numerical modeling. It is shown that partial transmittance of radiation in amorphous quartz balls bed provides for 2–5% increase in heater radiative efficiency in comparison with opaque material of carcass. In conditions of elevated ambient temperatures (as in, e.g., thermal kilns etc.), the increase in efficiency is smaller. It is shown that the transparency of porous media may not only decrease but, unexpectedly, increase maximum solid temperatures in comparison with the opaque one, in the case of big system size and high flow rate. In the later case, superadiabatic temperature excess (50–150 K) can be obtained in a solid phase. Also, some models of porous media optical properties are discussed.

1. Introduction

Investigations of the gas filtration combustion (FC) has rather long history, beginning from investigations of surface burning and heat recuperation in the first half of 20th century made by M. Ravich, G. Shwank and other scientists. Weinberg's concept of the 'excess enthalpy flame' [1], initiated a new wave of FC investigations directed to combustion of very lean fuels at 'superadiabatic' temperatures. Substantial theoretical and experimental researches were performed on thermal wave propagation in catalysts beds [2,3], application of FC to glass-wool production, other technical and ecological problems [4]. General properties of FC waves were investigated in a set of works [2–4]. Echigo [5] first emphasized the role of radiation transfer for heat recuperation in the system of porous plates. In the last years, FC investigations directed to more complicated systems characterized by non-stationary combustion and/or specific geometry and design of the systems. Search of new applications is also continuing. Recently, considerable activities were directed to design of heaters based on FC of gases for thermo-chemical treatment of metals, ceramics and other industrial needs. One possible geometry for such heaters is cylindrical or spherical, where reactants are filtered from center to periphery. The configuration provides flame stabilization inside porous body as a result of gas velocity diminishing with distance from symmetry center. The optical properties of the porous media may effect efficiency and other important parameters of the heater. Although the factor of radiation transfer in porous media was considered in many works dedicated to FC [6,9], there is no work analyzing the effect of the porous media optical properties on main parameters of the spherical and cylindrical radiative heaters. The aim of this work is to investigate it quantitatively via nu-

* Corresponding author.

0017-9310/00/$ - see front matter
PII: S0017-9310(99)00320-8

Nomenclature

T	temperature
T_0	ambient temperature
ΔT	temperature increment relative to T_0
T_{ad}	theoretical temperature of a mixture
ΔT_1	superadiabatic gain ($\Delta T_1 = T_{max} - T_{ad}$)
G	gas mass flow rate
y	normalized concentration of fuel
$W(y, T)$	chemical reaction rate
$Q = c_g \Delta T_{ad}$	reaction heat release
U	activation energy
z	preexponential factor
c	heat capacity
m	carcass porosity
d_0	diameter of porous carcass grain
u_g	local filtrational speed
L	average pore size
c_0	speed of light
$\boldsymbol{q}$	radiation energy flux vector
l_0	photon free path
Tr	normalized transmission for porous media layer
H	filling length
U	radiative energy density
r	radial coordinate
λ'	wavelength
λ'_{max}	emission wavelength corresponding to the maximum intensity
κ, a, s	extinction, absorption and scattering coefficients
α	volumetric heat transfer coefficient
λ	thermal conductivity
ρ	density
σ	Stephen–Boltzmann's constant
ε	integral emissivity
η	radiative efficiency

Subscripts

g	gas phase
s	solid phase
max	maximum
0	internal radius
1	localization radius
2	external radius

merical simulation and reveal possible effects of partial transparency of the porous media on the main parameters of conceptual cylindrical and spherical filtration combustion heaters (FCHs).

2. Optical properties of porous media

Optical properties of packed beds depend on material of bedding, grain surface structure and geometry of pores. Such materials as silicium carbide, asbestos are characterized by high absorptivity. There are many new ceramic materials (produced of SiO_2, Y_2O_3, MgO, ZrO_2 and other oxides) that have good transparency for optical and near IR radiation. The best transparent ceramics are based on Y_2O_3. Quarts glass and high density alumina (Al_2O_3) are characterized with high transparency for optical and near IR radiation and sharp decrease of transmittance at wavelength $\lambda' \cong 2.7$ μm for quartz and $\lambda' \cong 3$ μm for Al_2O_3. Absorption change and bias of the border wavelength with temperature is negligibly small, at least for the temperatures below $T = 1200°C$. More detailed information about thermal and optical properties of ceramics can be found in [7,8].

There are two basic approaches for modeling of the radiative transfer in Porous Media (PM): (1) detailed radiation modeling considering the interphase boundary conditions for radiation intensities, and (2) volume-averaged one, which assumes porous media to be a quasi-homogeneous media characterized by mean absorption and scattering coefficients. The first method is too heavy for calculation, the second one is widely used for radiative heat transfer calculation, although the theoretical foundations for its application are not completely investigated.

Conventional practice of volume-averaged modeling includes [9] determination of a representative volume of PM and scattering cross-section calculation for the unit by Mie's theory or (and) other methods. It is assumed that:

1. the local thermal equilibrium occurs;
2. no interference happens between scattering waves; and
3. each representative volume scatters as if it were alone, i.e. point (or independent) scattering occurs [9–11].

Assumption (2) leads to a limit on the minimum value of average interparticle clearance (pore size) L: $L/\lambda' > 0.5$ [10,11], where λ' is a wavelength. Obviously, packed beds made of big particles satisfy this condition. Although the third assumption implies limitations on intergranular spacing, it is suggested in [12] that the point scattering assumption is not crucial to the model.

Hottel et al. [10] have defined that independent scat-

Table 1
Photon free path l_0 measured via packing transmission and obtained by fitting of Chen and Churchill's experimental data [16]

Bedding material	d_0 (mm)	m	L (mm)	l_0 (mm)
Crashed quartz	4	0.42	3.3	4.1
Hollow Al_2O_3 balls	3	0.38	2.5	3.8
Solid Al_2O_3 balls	2.8	0.38	2.3	2.3
Solid Al_2O_3 balls	5.6	0.38	4.7	5.3
Borosilicate balls, $T_0 = 1366$ K	5	0.38	4.25	25[a]
Borosilicate balls, $T_0 = 1366$ K	5	0.38	4.25	9[a]

[a] Fitted by using experimental data [16].

tering takes place at considerable porosity of porous body $m > 0.73$. Kaviany [9] has defined that an assumption of independent scattering is well satisfied for semitransparent beds (grain optical thickness $\tau \cong 0.1$), whereas for opaque beds this assumption is substantiated for highly porous systems and porosity being $m = 0.4$, this assumption can lead to multiple overrating of porous body's transmittance. Such behavior is explained by multiple scattering caused by available surrounding particles. Regardless of the fact that conclusions of various works concerning the conditions of fulfilling assumptions (2) and (3) differ quantitatively, their qualitative content is the same. The question of local thermodynamic equilibrium of porous body's component is not discussed in above mentioned works, though at strong temperature gradients in porous media that occur in filtration combustion front, it is not fulfilled. Another problem is the difficulty of representative volume scattering calculation even for equal spherical balls bedding due to, first of all, complicated porous microstructure of real ceramics. In relation to the above statement, experimental definition of averaged optical characteristics of porous body as well as using rough models of optical properties, if acceptable, are rational.

Assume the porous body to be a pseudo-homogeneous medium characterized by extinction κ, absorption a and scattering s coefficients, $\kappa = a + s$. Neglecting absorption in gas phase, an average photon free path l_0 is equal, for opaque beds, to the average size of pores L and can be estimated from dimensional representation consideration as

$$l_0 = L = d_0 \sqrt[3]{m/(1-m)}, \tag{1}$$

here m is the porosity, d_0 the characteristic diameter of bedding granule, although other relations obtained for different types of porous materials can be found in literature [13,14]. For a given emissivity of carcass material (albedo or related parameters), effective absorption and scattering may be estimated

$$a = \varepsilon/L, \qquad s = (1-\varepsilon)/L, \tag{2}$$

where ε is the integral emissivity factor of carcass material.

For transparent (semi-transparent) beds, photon free path is longer than average pore size, though radiation scattering is rather high due to diffraction, refraction and interference of beams. In practice, it is worth to calculate by using Mie's theory or geometrical optics [9,15], under the following conditions:

1. photon free path in individual bedding substance considerably (by a factor of 3 or more) exceeds the length of pore space;
2. pellet surface is smooth and low-scattering;
3. packing pellets have uniform shape and size.

Otherwise, it is worth to roughly evaluate PM scattering coefficient s and consider

$$a = (1-m)a_s, \qquad \kappa = s + (1-m)a_s \tag{3}$$

where a_s is the absorption factor in individual substance of solid phase, m is the carcass porosity.

For transparent fillings scattering can be omitted from Eq. (3) as a consequence of negligible reverse scattering on transparent particles (lower by an order of magnitude in comparison with opaque ones [16]) as well as the fact that scattered part of emission actually does not participate in energy transfer on considerable optical thickness [15].

Some data obtained by measuring photon average free path is shown in Table 1. For the purpose, samples of porous media were prepared of quartz grains of irregular shape, hollow and solid balls of opaque Al_2O_3. Laboratory 0.62 μm He–Ne laser was used as the radiation source. Photometer was used as a detector. Packing layer thickness was varied from 0.5 to 1 cm for solid balls and from 1 to 2.5 cm for hollow balls and quartz.

As follows from the data in Table 1, photon free path length in the bedding of quartz and hollow Al_2O_3 balls is higher than typical pore size, which is explained by transmittance of the bedding. However, this difference is not large due to intensive scattering at rough Al_2O_3 balls and quartz grains of irregular shape.

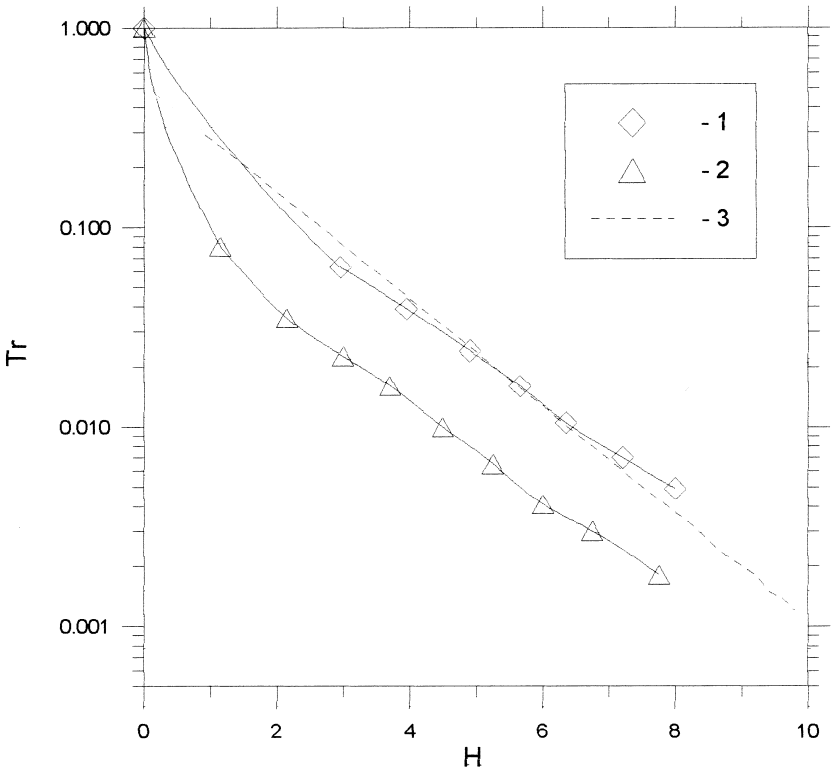

Fig. 1. Normalized integrated transmission Tr of a filling composed by Bsi-glass spheres $d_0 = 5$ mm. H: porous layer length (cm). Experimental data by Chen and Churchill [16]; (1) source temperature $T_0 = 1366$ K, (2) 922 K, (3) differential approximation calculations for $l_0 = 5d_0$ (case 1).

Considerable radiation transmittance is typical for packed beds of near-spherical grains with smooth (polished) surface. Estimation based on differential approximation (DA) for radiative transfer using the experimental data of Chen and Churchill [16], obtained for packed beds made from 5 mm Bsi-glass spheres, gives effective photon free path by a factor of 5 more than the pore size, according to Eq. (1) (Fig. 1).

From the data in Fig. 1, it can also be seen that integrated transmittance is significantly effected by dependence of a photon free path on emission wavelength (e.g. IR transmittance with maximum intensity on $\lambda'_{\max} = 2.1$ μm (corresponding to $T_0 = 1366$ K) by a factor of 3 that exceeds for $\lambda'_{\max} = 3.1$ μm ($T_0 = 922$ K)). So it can be predicted that temperature distributions and performance characteristics of FCH will be significantly changed depending on particle size and porous media material (the later defines optical characteristics).

3. Mathematical problem formulation

We consider here a one-dimensional cylindrical system (Fig. 2). It will be assumed that gas phase is optically transparent and isobaric, and overall heat release is described by Arrhenius Brutto-reaction.

Mathematical model of FCH consists of energy balance equations for solid and gas phases and mass balance equation for limiting component. Neglecting diffusion and thermal conductivity in comparison with conduction in the gas phase, it will be defined as follows:

$$c_s\rho_s\frac{\partial T_s}{\partial t} = \frac{1}{r}\frac{\partial}{\partial r}\lambda r\frac{\partial T_s}{\partial r} - \nabla \boldsymbol{q} + \alpha\left(T_g - T_s\right), \tag{4}$$

$$c_g\rho_g u_g\frac{\partial T_g}{\partial r} = -\alpha\left(T_g - T_s\right) + QW\left(y, T_g\right), \tag{5}$$

$$\rho_g u_g\frac{\partial y}{\partial r} = -\rho_g W\left(y, T_g\right). \tag{6}$$

$$W\left(y, T_g\right) = yz\exp\left(-15{,}640/T_g\right), \tag{7}$$

$$\rho_g T_g = \text{const}, \tag{8}$$

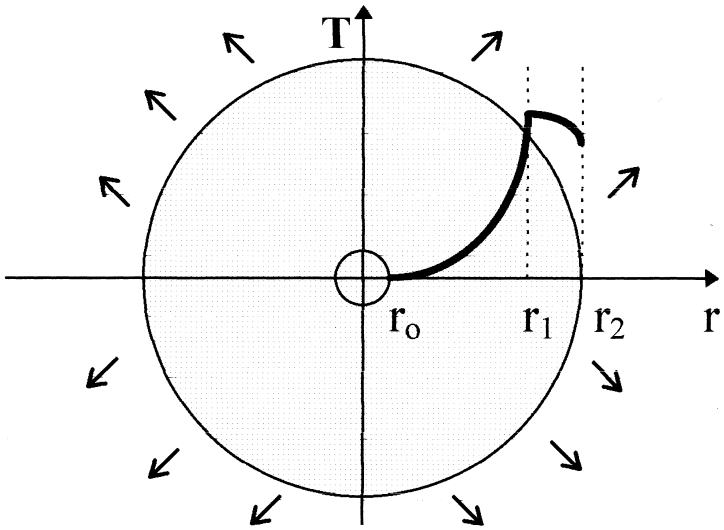

Fig. 2. Sketch of axially symmetric FCH. Carcass temperature profile is shown by solid line, products and irradiation by arrows.

$$\nabla\left(\frac{1}{a+s}\right)\nabla U - 4aU + 16a\sigma T_s^4/c_0 = 0 \tag{9}$$

$$\nabla q = 4a\sigma T_s^4 - c_0 aU \tag{10}$$

where Eqs. (9) and (10) describe differential approximation for radiative heat transfer. The set of governing equations is coupled with the following boundary conditions for Eqs. (4)–(6) and (9):

$$\frac{\partial T_s}{\partial r}|_{r_0} = 0, \quad \frac{\partial T_s}{\partial r}|_{r_2} = 0; \quad T_g|_{r_0} = T_0; \quad y|_{r_0} = 1;$$

$$\frac{\partial U}{\partial r}|_{r_0} = 0, \quad |\boldsymbol{q}\|_{r_2} = \frac{c_0}{2}U|_{r_2}.$$

Input energy in the FCH is defined by flow rate and the heat content of mixture composition $Q^+ = GQ$ and redistributed by radiation emission and combustion products: $Q^+ = Q_{rad} + c_g G \Delta T_{2,g}$.

Radiative efficiency, defined as a ratio of radiation energy emitting from the heater surface to the total input energy, can be presented in the form:

$$\eta \equiv \frac{Q_{rad}}{Q^+} = 1 - \frac{\Delta T_{2,g}}{\Delta T_{ad}}, \tag{11}$$

where $\Delta T_{2,g}$ is the combustion products temperature rise (at exit) above ambient temperature.

The system of Eqs. (4)–(10) with the corresponding boundary conditions was approximated by finite differences and solved iteratively by sweep method (forming three-diagonal matrix for Eqs. (4) and (9) and integrating Eqs. (5) and (6) explicitly). The calculations were done primarily for methane–air mixtures with fuel concentrations corresponding to the adiabatic temperatures (as excess above surroundings) $\Delta T_{ad} = 1200$ and 2000 K. The mass flow rate $G = 2\pi r \rho_s u_g$ (for 1 m of the heater length) was varied in the wide range $G = 0.001$–2.5 kg/(s m). It was done to model systems with external radius $r_2 = 10$ and 25 cm. The carcass thermal conductivity coefficient was chosen constant with other parameters as follows: $\lambda = 1.5$ W/(m K), $m = 0.4$, $d_0 = 5.6$ mm, $r_0 = 1$ cm, $c_g = 1.3 \times 10^3$ J/(kg K), $c_s = 1.3 \times 10^3$ J(kg K), $\rho_s = 2.5 \times 10^3$ kg/m^3. Interphase heat exchange coefficient α was defined according to [17]. Calculations were carried out for porous media formed by highly transparent pellets (smooth quartz spheres) and rather opaque ones (Al_2O_3 spheres with rough surface). Absorption and scattering coefficients for Al_2O_3 were estimated from Eqs. (1) and (2) with $\varepsilon = 0.6$. Absorption coefficient for quartz filling was defined according to the data for BSi-glass [16], neglecting scattering.

As a result of the calculations, radiative efficiency (according to Eq. (11)), maximum solid temperature and reaction zone localization (defined as the maximum gas phase temperature point) was obtained. As reported in [18], reaction front localization in the systems of such geometry may depend on combustion initiation place (e.g. at the entrance or exit). To avoid such uncertainty, ignition near the entrance was chosen for all simulations.

Data for FCH radiative efficiency for the cases of transparent and opaque fillings as a function of flow rates, mixture heat content and system size (external radius) are combined in Fig. 3 (here, and in the follow-

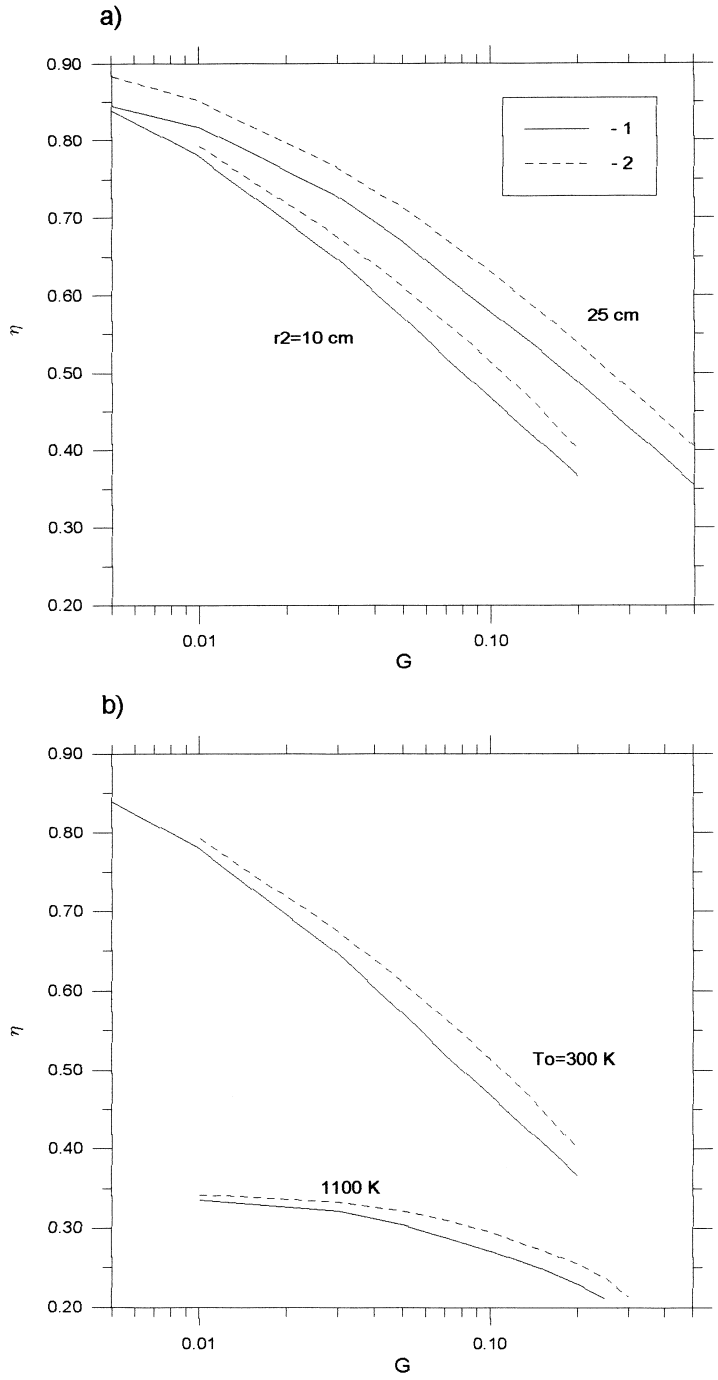

Fig. 3. Cylindrical FC heater radiative efficiency dependency on flow rate, G (kg/(s m)), for different porous layer transparency: (1) rough Al_2O_3 spheres $d_0 = 5.6$ mm, (2) polished quartz spheres 5.6 mm; (a) $\Delta T_{ad} = 1200$ K, $r_2 = 10$ and 25 cm; (b) $\Delta T_{ad} = 1200$ K, $r_2 = 10$, $T_0 = 300$ and 1100 K.

ing figures the highest value of flow rate corresponds to the blow-out limit of heater operation). As it follows from the results, radiative efficiency for transparent porous media is higher than that for the opaque one. Degree of this excess $\Delta\eta$ is slightly dependent on external radius value, and has a more significant dependence on fuel heat content (or ΔT_{ad}). Maximum attained values of $\Delta\eta$ are shown in the Table 2. $\Delta\eta$ is slightly rising with increase in the flow rate, has not a well resolved maximum and decreasing when reaching maximum possible flow rate (Fig. 3a,b). For elevated ambient temperatures (as in thermal kilns), it has characteristically less values for radiative efficiency.

Data obtained for maximum carcass temperatures for transparent and opaque materials are collected in Fig. 4. From these results it follows that maximum temperature $T_{s,\,max}$ of a transparent carcass is on average 50–150 K lower than that for the opaque one. For mixtures with less fuel concentrations, this discrepancy is higher. As it follows from the results shown in Fig. 4, maximum temperatures for the transparent packings rather than opaque ones become less divergent from each other with increase in the flow rate, heat content and FC heater sizes, and for larger radius ($r_2 = 25$ cm) even 'inversion' takes place, i.e. $T_{s,\,max}$ for transparent packing overcomes $T_{s,\,max}$ for opaque one. This effect can be attributed to the fact that increase (in comparison with opaque material) of radiative heat loss from reaction zone is also coupled with elevation of upstream heat transfer. The latter enhances heat recuperation and leads to an increase of maximum solid phase temperature and upstream shift of flame front position. The relative competition of the upstream heat transfer and radiative heat losses results in the following trends as a function of mixture heat content, FC heater sizes and other parameters (Fig. 4): e.g. for $r_2 =$ 10 cm and $T_0 = 300$ K, the maximum temperature for transparent media is lower than that for opaque media for arbitrary flow rates. On the contrary, for $T_0 =$ 1100 K, this 'inversion' takes place for the highest (near blow-out limit) flow rates (Fig. 4b).

As it can be seen from Fig. 5, for small flow rates combustion front is localized further from the symmetry axis for transparent packings than for the opaque ones, due to excessive radiation losses in an upstream direction. With an increasing flow rate, this can be maintained or changed by an opposite one, as a consequence of intense radiation heat flux which enhances thermal recuperation in a system. Maximum temperature 'inversion' corresponds to the system operation regimes where combustion front localization occurs significantly closer to the system axis for a transparent media rather than for an opaque one (Fig. 5).

It should be noted that maximum attained solid temperatures are increasing with the rise in flow rate G. Slight decrease in temperature dependence on flow rate takes place only in the immediate vicinity of blow-out limit, e.g., $G > 0.2$ kg/s in Fig. 6a.

It should be emphasized that the presence of radiation (photon free path $l_0 = 5d_0 = 28$ mm) under given conditions can lead to the over adiabatic heating of the solid body (see, e.g. Fig. 4a, region $G >$ 0.2 kg/s, $r_2 = 25$ cm). For such case, some surplus (50–100 K) is characteristic for solid temperature above theoretical temperature of the mixture $T_{ad} = T_{ad} + T_0 = 1500$ K. The fact that the phenomenon is a consequence only of the radiative transfer was confirmed directly by calculations for the adiabatic case (i.e. without emission from external surface). For this purpose, photon free path was varied from $0.1d_0$ to $5d_0$, which resulted in change in temperature excess value from 0 to 150 K, correspondingly, and the shape of the solid temperature profile changed from the monotonous 'S'-shape with $T_{max} = T_{ad}$ to that with characteristic 'peak' in the combustion region. This effect should be attributed to the 'far-range' heat recuperation via radiation from distributed high-temperature layers placed downstream to the preheated zone. The phenomenon is analogous to the effect reported in the work [5] by Echigo et al., where superadiabatic effect achieved in two highly porous plates

Table 2
Maximum excess efficiency $\Delta\eta$ of cylindrical FCH calculated for transparent quartz balls packing in comparison with opaque Al_2O_3 balls packing

r_2 (cm)	ΔT_{ad} (K)	T_0 (K)	G (kg/(s m))	$\Delta\eta$ (%)
10	1200	300	0.1	4.7
25	1200	300	0.1–0.2	5.1
10	1200	1100	0.15–0.2	2.5
25	1200	1100	0.45	2.5
10	2000	300	0.5	5.5
25	2000	300	0.5	5.9
10	2000	1100	0.5	4.8
25	2000	1100	1.5	5

Table 3
Porous media maximum solid temperature and superadiabatic gain ΔT_1. Quartz and yttrium glass are treated as having free photon paths $l_0 = 5d_0$ and $l_0 = 15d_0$ respectively. [The provided data are optimized (for maximum values) as a function of mass flow rate: $G = 0.1$ kg/s ($r_2 = 25$ cm) and $G = 0.6$ kg/s ($r_2 = 50$ cm) $d_0 = 5.6$ mm.]

Radius (cm)	25	50
$T_{max}/\Delta T_1$ (K) (quartz glass packing)	1340/40	1390/90
$T_{max}/\Delta T_1$ (K) (yttrium glass packing)	1320/20	1480/180

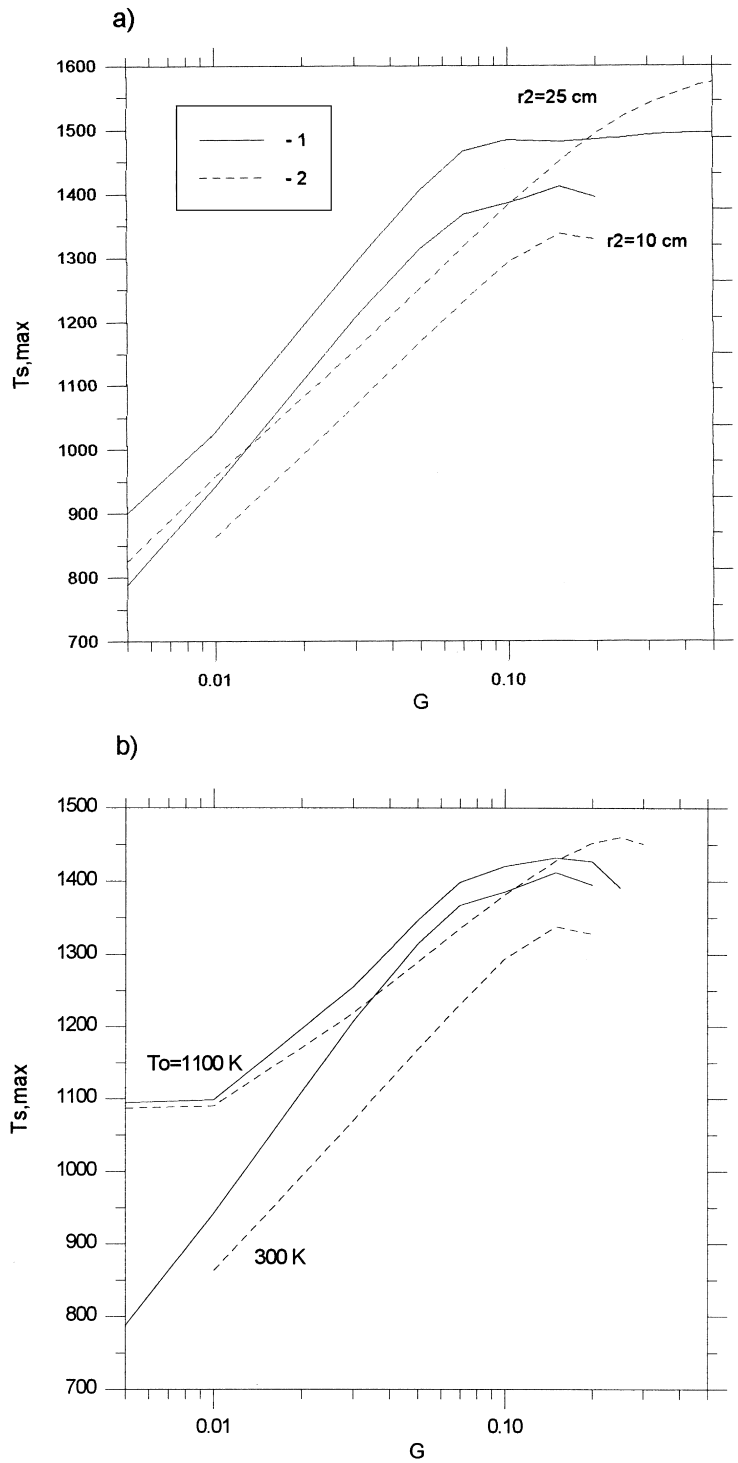

Fig. 4. Cylindrical FC heater maximum solid temperature $T_{s,\,max}$ K dependence on flow rate, G (kg/(s m)), for different porous layer transparency: (1) rough Al_2O_3 spheres $d_0 = 5.6$ mm, (2) polished quartz spheres 5.6 mm; (a) $\Delta T_{ad} = 1200$ K, $r_2 = 10$ and 25 cm; (b) $\Delta T_{ad} = 1200$ K, $r_2 = 10$, $T_0 = 300$ and 1100 K.

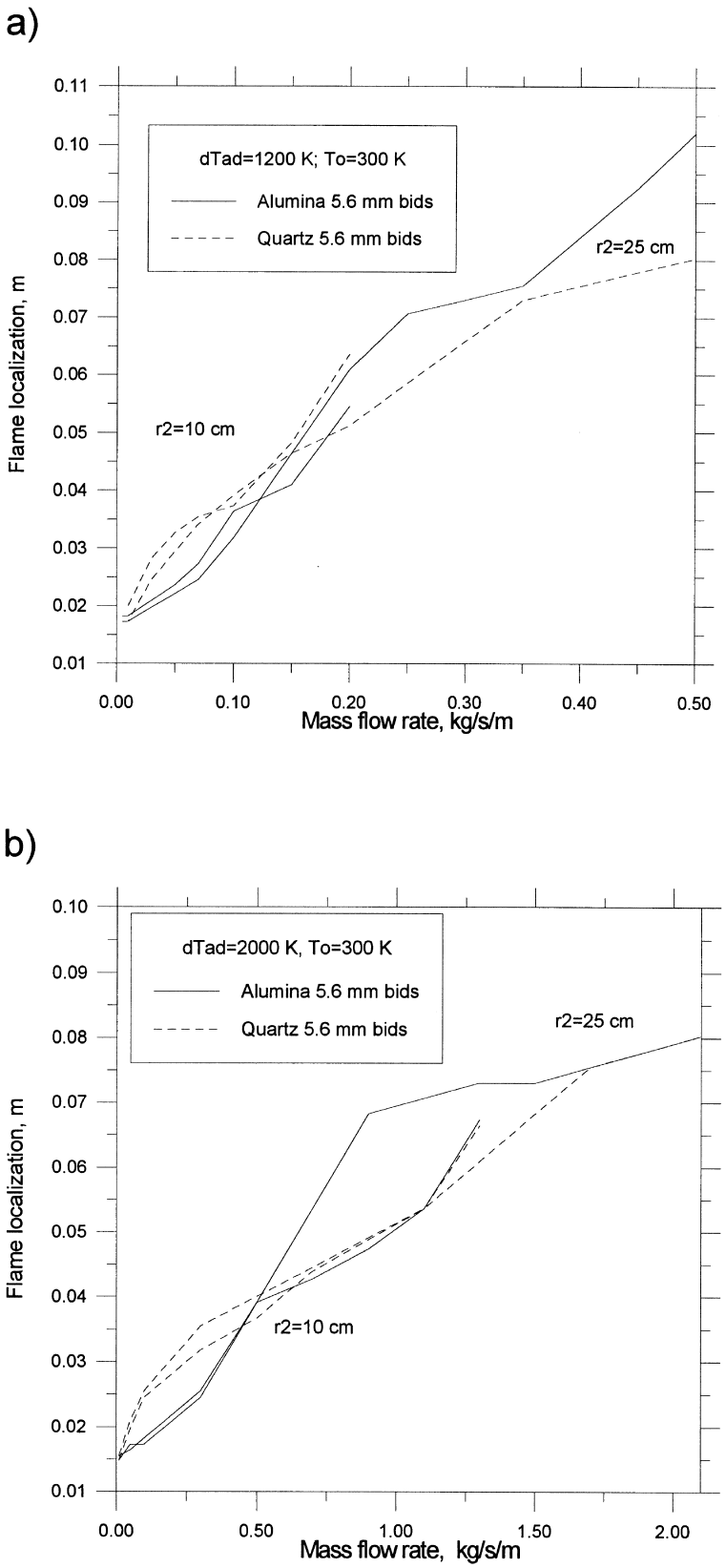

Fig. 5. Cylindrical FC heater stabilization radius r_1 (m), dependence on flow rate, G (kg/(s m)), for different porous layer transparency: (1) rough Al_2O_3 spheres $d_0 = 5.6$ mm; (2) polished quartz spheres 5.6 mm; (a) $\Delta T_{ad} = 1200$ K, $r_2 = 10$ and 25 cm, (b) $\Delta T_{ad} = 2000$ K, $r_2 = 10$ and 25 cm.

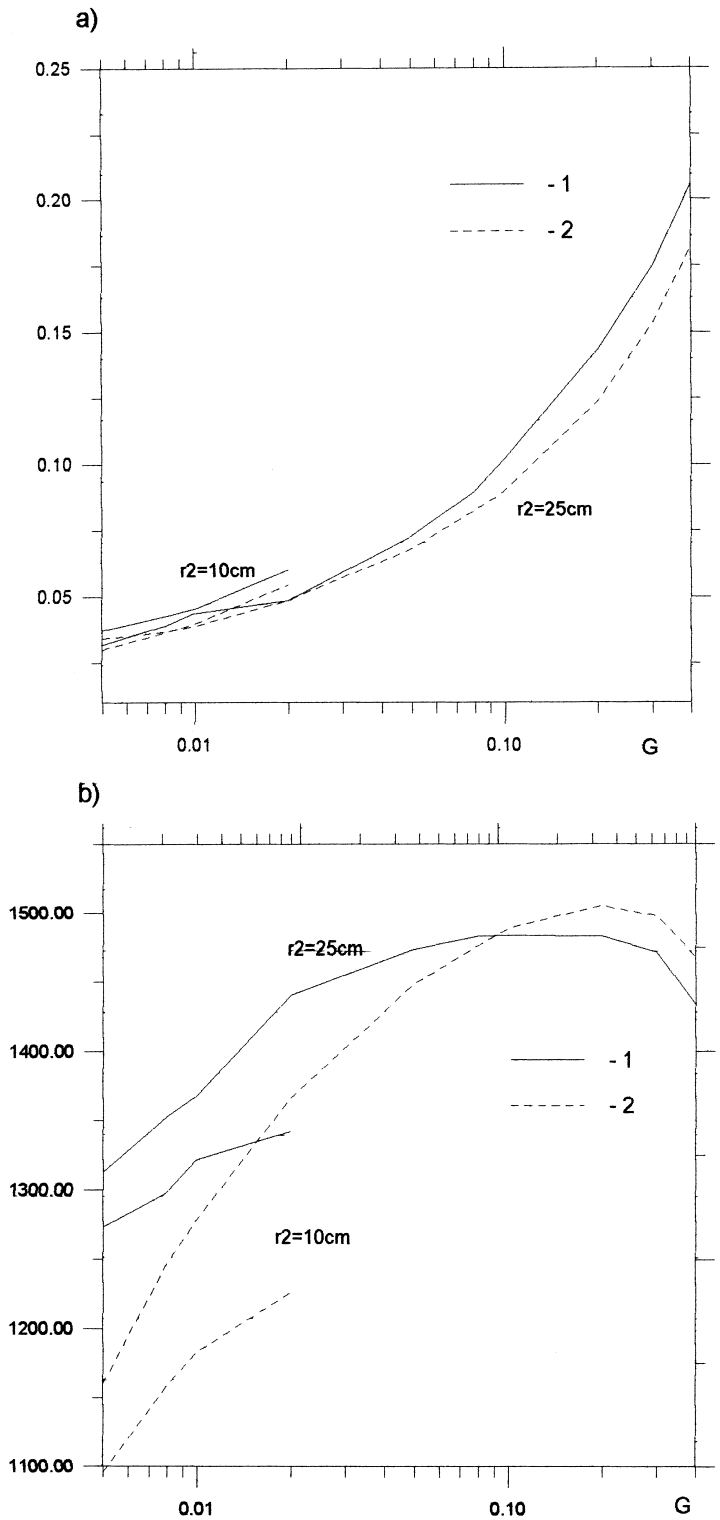

Fig. 6. (a) Spherical FC heater stabilization radius r_1 dependence on flow rate, G (kg/(s m)), for different porous layer transparency: (1) rough Al_2O_3 spheres $d_0 = 5.6$ mm, (2) polished quartz spheres 5.6 mm ($\Delta T_{ad} = 1200$ K, $r_2 = 10$ and 25 cm), (b) maximum temperature of the solid $T_{s,\,max}$, K as a function of flow rate, G.

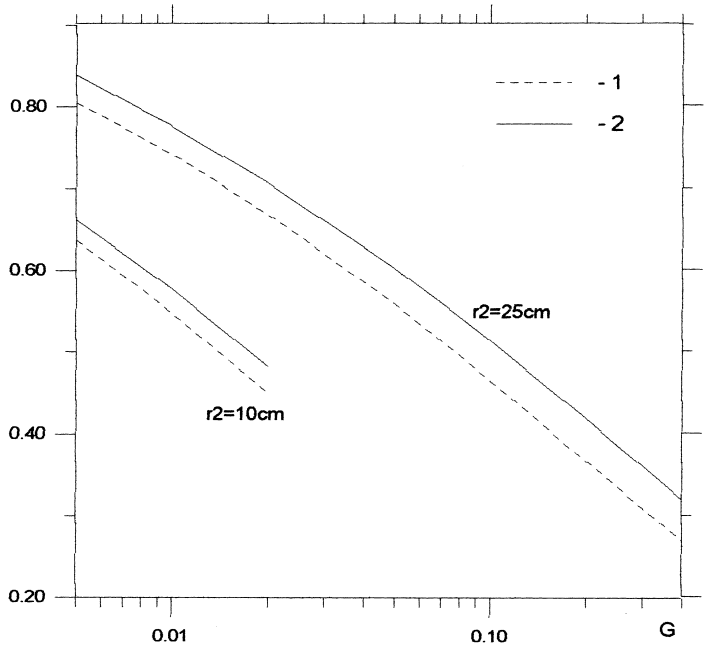

Fig. 7. Spherical FC heater radiative efficiency dependency on flow rate, G (kg/(s m)), for different porous layer transparency: (1) rough Al_2O_3 spheres $d_0 = 5.6$ mm, (2) polished quartz spheres 5.6 mm ($\Delta T_{ad} = 1200$ K, $r_2 = 10$ and 25 cm).

was investigated. In the study, approximately the same excess values (near 100 K) in the solid temperatures were observed.

Spherical type FCHs were analyzed similar to the cylindrical one. For this purpose, only Laplacians in governing the Eqs. (4)–(10) were respectively changed. Radiative efficiency, maximum solid temperature and stability radius are presented in Figs. 6 and 7 (in the case the system parameters are: $G = \pi r^2 \rho_g u_g$ $T_{ad} =$ 1200 K, $r_2 = 10$, 25 cm, $r_0 = 1$ cm, $T_0 = 300$ K).

Porous carcass maximum temperature and superadiabatic gain, defined as $\Delta T_1 = T_{max} - T_{ad}$, for the spherical systems (including surface emission) with external radius 25 and 50 cm are shown in Table 3. It should be noted that superadiabatic excess temperature rises with the system sizes. More detailed discussion concerning flame localization in cylindrical and spherical systems can be found in [18].

4. Conclusions

Usage of the transparent fillings with a photon free path several times higher than the pore size makes it possible to enhance FCH radiative efficiency by 2–5% for considered system parameters and normal ambient temperature. For elevated ambient temperature, that is intrinsic, e.g., to thermal kilns, excessive value of radiative efficiency is almost vanishing for low flow rates (Fig. 3). By using transparent beds, it is possible to lower the maximum temperature attained in carcass by 50–150 K for the given conditions. However, for the systems with large external radius ($r_2 > 10$ cm for the chosen parameters), as a consequence of increased recuperation efficiency, it is possible to obtain the opposite effect, i.e. transparent media gives higher temperatures (Fig. 4). The latter can result in superadiabatic solid temperatures. It is worth mentioning that solid body superadiabatic temperature in stationary conditions is principally achievable only via radiation.

Spherical geometry heaters are characterized by qualitatively the same trends for maximum solid temperature, radiative efficiency and stabilization radius dependencies on flow rate, as the cylindrical one. It should be noted also that effective enhancement of thermal recuperation in transparent porous media can be used for the improvement of superadiabatic combustion regimes.

References

[1] F.J. Weinberg, Nature 233 (1971) 239–241.
[2] Yu. Sh. Matros, Rasprostranenie teplovyuch voln v geterogennyuch sredach, Novosibirsk, 1988 (in Russian).
[3] H.-K. Rhee, R.P. Lewis, N.R. Amundson, Ind. Eng. Chem. Fundam. 13 (1) (1974) 1–4.

[4] J.R. Howell, et al., Progress in Energy and Combustion Science 22 (1996) 122–145.
[5] R. Echigo, Y. Yoshizawa, K. Hanamura, T. Tomimura, in: Proc. of the Int. Heat Transfer Conference, San Francisco, vol. 2, 1986, pp. 827–832.
[6] S.B. Sathe, R.E. Peck, T.W. Tong, Int. J. Heat Mass Transfer 33 (6) (1990) 1339–1346.
[7] V.P. Balkevich, Technicheskaya keramika, Moscow, 1984 (in Russian).
[8] R.E. Krzhizhanovskii, Z. Yu. Shtern, Teplofizicheskie svoistva nemetalicheskich materialov (okislyu), Leningrad, 1973 (in Russian).
[9] M. Kaviany, Principles of Heat Transfer in Porous Media, New York, 1991.
[10] H.C. Hottel, A.F. Sarofim, W.H. Dalzell, I.A. Vasalos, AIAA J. 9 (1971) 1895–1899.
[11] Y. Yamada, J.D. Cartigny, C.L. Tien, ASME J. Heat Transfer 108 (1986) 614–620.
[12] M.Q. Brewster, C.-L. Tien, ASME J. Heat Transfer 104 (1982) 573–579.
[13] N.V. Pavlyukevich, Inzenerno — Phizicheskii Zhurnal 59 (4) (1990) 606–609.
[14] J.D. Verschoor, P. Greeber, Trans. ASME 74 (1952) 961–968.
[15] R. Ziegel, J. Howell, Theploobmen izlucheniem, Moscow, 1975, p. 934 (in Russian).
[16] J.C. Chen, S.W. Churchill, AIChE Journal 9 (1) (1963) 35–41.
[17] M.E. Aerov, O.M. Todes, D.A. Narinskii, Apparatyu so statsionamyum zernistyum sloem, Moscow, 1979 (in Russian).
[18] K.V. Dobrego, S.A. Zhdanok, S.I. Futko, Int. J. Heat Mass Transfer, 41 (1998) 3647–3655.